Available online at www.sciencedirect.com

ScienceDirect

Science and Technology of Materials

http://ees.elsevier.com/stmat

Science and Technology of Materials 30 (2018) 109–119

Advanced liquid state processing techniques for ex-situ discontinuous particle reinforced nanocomposites: A review

C. Kannan *, R. Ramanujam

School of Mechanical Engineering, VIT University, Vellore 632 014, India

Received 10 December 2017; accepted 3 May 2018

Abstract

Recent times, metal matrix composites (MMC) are considered as candidate materials for numerous applications such as aerospace, automotive and military industries due to improved properties over the conventional metals and alloys. Out of the different categories of metal matrix composites, discontinuous particulate reinforced composites are preferred for industrial applications due to low manufacturing cost. High fracture toughness, improved ductility and machinability characteristics support the selection of metal matrix nanocomposites (MMnC) over conventional composites for different applications. The majority of nanocomposites are produced through liquid state processing due to faster processing time and economy. However, the conventional liquid processing method leads to poor wetting of reinforced nanoparticles by molten metal that degrades the quality of the fabricated nanocomposite. This paper reviews some of the advanced liquid state processing techniques adopted for the improved wettable characteristics of nanoparticles and their uniform distribution in the metal matrix.

Keywords: Nanocomposites; Ultrasonic assisted cavitation; Compocasting; Rheocasting; Squeeze casting; Thixoforming

1. Introduction

At present, metal matrix nanocomposites are being manufactured by employing either a solid state or liquid state processing method [1]. However, the latter is preferred over the former due to inherent cost-effectiveness [2–5]. In liquid state processing, the nano-reinforcements can be either added to the melt from outside (ex situ) or produced inside the melt through reactive processing (in situ). The techniques such as stir casting, infiltration, disintegrated melt deposition and high pressure die casting fall into ex situ category [6], while liquid gas bubbling is under in situ category [7].

Nevertheless of merits, a major threat to the practical implementation of the liquid state processed nanocomposite is the agglomeration of particles during its fabrication. This agglomeration is associated with the poor wettable characteristics of the particles. In general, wettability represents the extent of intimate contact between a liquid and solid. The bonding force between the liquid and solid phase can be expressed in terms of surface tension and the contact angle of the liquid. The magnitude of contact angle (θ) describes the type of wettability. Perfect wetting is attained when $\theta = 0^\circ$ and no wetting took place for $\theta = 180^\circ$. Partial wetting is accounted for $0 < \theta < 180^\circ$ [8]. The contact angle for different ceramic reinforcements is presented in Table 1.

To improve the wettability of reinforced particles, several approaches have been attempted [16–18] viz. (i) a coating on reinforced particles, (ii) a suitable treatment on reinforced particles and (iii) the addition of alloying elements to the matrix. All these techniques are based on either increasing the surface energy of reinforced particles or decreasing the surface tension of liquid matrix and particle–matrix interfacial energy [19]. Non-addressing of this wettability issues will lead to a non-uniform distribution of nanoparticles in the base matrix [20].

For the fabrication of nanocomposites, the reinforcements may be added into the matrix in different forms like particulates, whiskers, fibres and nanowires. However, manufacturing easiness and low-cost favour the particle reinforced composite over whisker-reinforced [21,22]. In addition, isotropic properties of

* Corresponding author.
E-mail address: kannan.chidambaram@vit.ac.in (C. Kannan).

https://doi.org/10.1016/j.stmat.2018.05.005

Nomenclature

Al_2O_3	aluminium oxide
PSN	particle stimulation nucleation
CTE	coefficient of thermal expansion
PTF	powder thixoforming
DRX	dynamic precipitation recrystallization
SC	squeeze casting
DSC	differential scanning calorimetry
SCHE	stir casting with hot extrusion
DUV	direct ultrasonic vibration
SEM	scanning electron microscopy
HPDC	high pressure die casting
SiC	silicon carbide
HPIC	high pressure infiltration casting
SL	semisolid–liquid
IUV	indirect ultrasonic vibration
SS	semisolid–semisolid
MMC	metal matrix composite
TF	thixoforming
MMnC	metal matrix nano composite
UAC	ultrasonic assisted cavitation
MWCNT	multi-wall carbon nano tubes
UTS	ultimate tensile strength
PM	powder metallurgy
YS	yield strength

Table 1
Contact angles between liquid aluminium and various ceramic reinforcements.

Reinforcement	Contact angle	Temperature	Reference
Graphite	140–160°	900 °C	[9]
SiC	150°	900 °C	[10]
Al_2O_3	90°	900 °C	[11]
B_4C	135°	900 °C	[12]
SiO_2	150	700 °C	[13]
Si_3N_4	164	700 °C	[14]
BN	160	900 °C	[15]

nanocomposite can be assured through uniform distribution of particles in the matrix. The reinforced ceramic particles might be from the category of oxides, borides and carbides. By inherent, these ceramic particles owe improved properties in terms of high hardness and mechanical strength at elevated temperatures, high stiffness, low density, low electrical/optical conductance and insulation properties [23].

Although quite a lot of solid state processing techniques such as powder metallurgy [24,25], flake powder metallurgy [26,27] and hot pressing [28] have been explored by the researchers around the world to achieve the uniform distribution of nanoparticles. The literature also reveals that only limited number of review articles is available on the reinforcing philosophies and characterization of liquid state processed nanocomposites [29–31] and limited elaboration on the advanced liquid processing techniques for nanocomposite fabrication. Hence, the current review strives to examine the influence of these processing techniques on the uniform distribution of nanoparticles, microstructural and mechanical characterization of nanocomposites. Further, the review comprehends the methodological and comparative analysis of these processing techniques. A comprehensive summary of various ex situ liquid processing techniques available for the production of nanocomposites is provided in Fig. 1.

2. Liquid processing of nanocomposites

Associated cost-effectiveness, simplicity and bulk manufacturing capability make the stir casting as one of the most preferred techniques for producing metal matrix composites [1,33–40]. The reinforcements are added and distributed in the matrix which is molten (liquid) state, using a mechanical stirrer. The melt along with the dispersed particles can be given the final shape by employing sand casting, permanent die casting and/or squeeze casting [41]. The conventional stir casting is usually associated with drawbacks such as (i) air entrapment due to rotating stirrer, (ii) undesired chemical reaction at the matrix/reinforcement interface, (iii) non-homogenous distribution of reinforced particles in the melt. All effects combined together deteriorate the end quality of the manufactured composites. Especially when nano-scale reinforcements are used, their tendency to agglomerate and forming nanoparticle clusters increases which further aggravates the non-uniform distribution [34,42,43]. In order to overcome the drawbacks of traditional stir casting, the innovative processing techniques adopted by different researchers are explained in the subsequent sections.

2.1. Ultrasonic assisted cavitation

Li and his co-workers [44–47] adopted the technique called ultrasonic assisted cavitation (UAC) for the uniform dispersion of silicon carbide (SiC) nanoparticles (Avg. particle size 30 nm) in the matrix of aluminium and magnesium alloys. A schematic representation of their experimental setup is shown in Fig. 2. The molten metal was produced inside a graphite crucible that was further connected to the electrical heating unit. A titanium waveguide coupled to a 20 kHz, 600 W ultrasonic transducer was dipped into the melt. The melt was protected by an inert gas. The melt temperature was continuously monitored using a temperature probe and maintained about 100 °C above the melting temperature of the base alloy. This was done to ensure the adequate flowability of molten metal inside the mold.

The high-intensity ultrasonic waves (magnitude higher than 25 W/cm^2) generated through an ultrasonic transducer are able to produce nonlinear effects such as transient cavitation and acoustic streaming in the melt [48–50]. These nonlinear effects are responsible for refining the microstructures, degassing of molten metal and dispersion of particles in the melt. The transient acoustic cavitation consists of positive and negative pressure cycle that extends for a time period of about 100 ms. Under the influence of high-intensity ultrasonic waves, thousands of microbubbles are formed and grow during the negative pressure cycle. These microbubbles are implosively collapsed during the positive pressure cycle which, in turn producing the

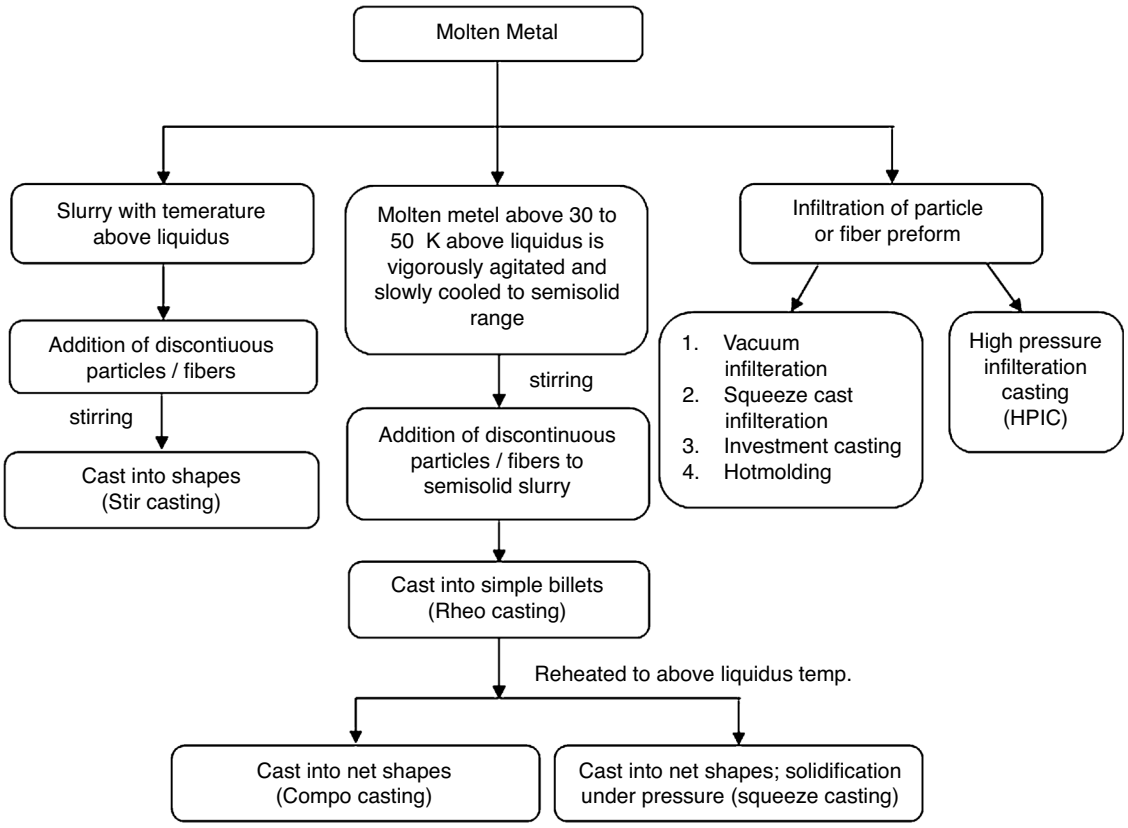

Fig. 1. Ex situ liquid processing methods for metal matrix nanocomposites [32].

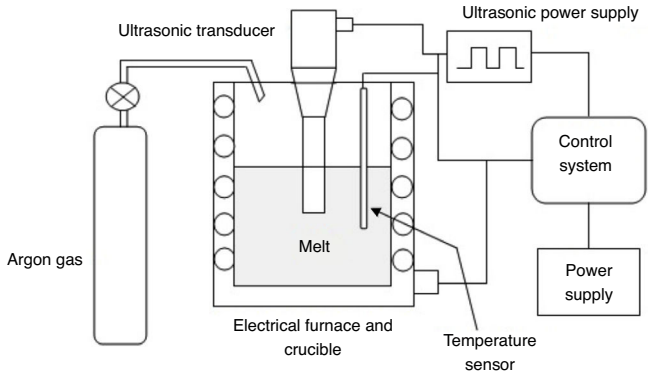

Fig. 2. A schematic of ultrasonic assisted cavitation technique [45].

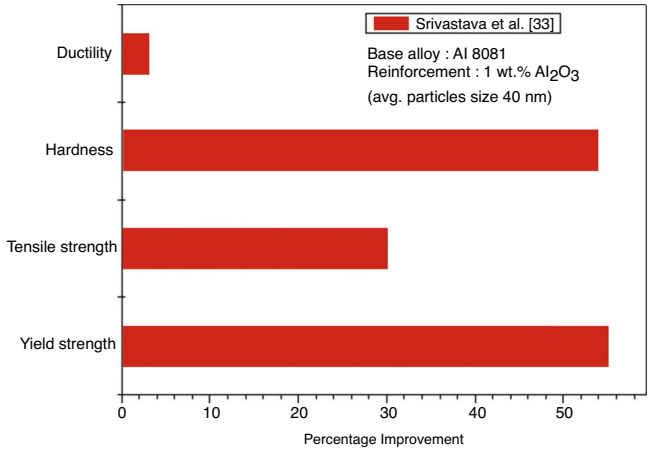

Fig. 3. Improved mechanical properties of UAC processed nanocomposite over unreinforced alloy [33].

micro-hotspots. These spots are characterised by extremely high temperatures (5000 °C) and pressures (1000 atm) and heating and cooling rates above 10^{10} K/s [51]. The implosive impact produced via transient cavitation is strong enough to break down the clusters of nanoparticles and uniformly disperse them in the molten metal. Improved wettable characteristics of nanoparticles can also be achieved with this short duration impacts coupled with high temperatures [52,53]. Thus, production of nanocomposites with a uniform distribution of particles [54–56] and reduced porosity [57,58] is almost possible. Al 6061 based nanocomposite (1 wt.% n-Al_2O_3) produced through ultrasonic assisted cavitation was found to possess enhanced mechanical properties over unreinforced alloy [54,59] and their percentage improvement is shown in Fig. 3.

The results of the tensile test performed on A356 alloy and its nanocomposites are presented in Table 2. The microstructural examination of these materials revealed that UAC is capable of breaking up the dendritic structures and forming the globular grain structures. Owing to this fact, UAC processed aluminium alloy and nanocomposites were found to possess superior mechanical properties over the conventional stir cast. With respect to nanocomposites, a mismatch in coefficient of

Table 2
Tensile test results for conventional and UAC processed A356 samples [55].

Material	Tensile strength (MPa)	Elongation (%)
Argon degassed A356 alloy	157.5 + 6.2	8 + 0.2
UAC processed A356 alloy	172.6 + 7.9	8 + 0.6
UAC processed A356 nanocomposite (A356-1% SiC)	172.0 + 5.9	4.3 + 0.5
UAC processed A356 nanocomposite (A356-1% Al_2O_3)	177.6 + 8.2	4.2 + 0.4

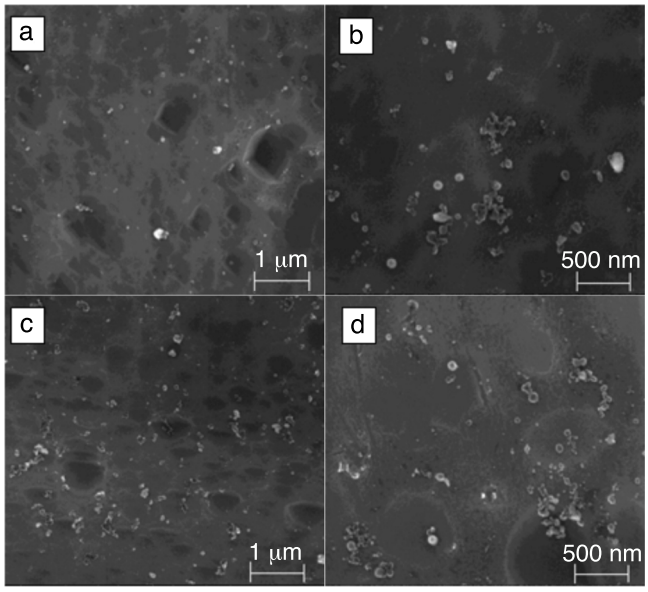

Fig. 4. SEM images of Al 6061 based nanocomposites with (a) 1 wt.% Al_2O_3, (b) 2 wt.% Al_2O_3, (c) 3 wt.% Al_2O_3, (d) 4 wt.% Al_2O_3 [54].

thermal expansion (CTE) between the matrix and reinforced particle dominates in strengthening the nanocomposites, which is followed by Orowan and Hall–Petch strengthening mechanisms [55,59]. Using UAC method, nanoparticle reinforcement of 4 wt.% or lower can be uniformly dispersed in the matrix without much complication. Beyond this weight percentage, the nanoparticles were observed to form clusters [54]. This can be inferred from the scanning electron microscope (SEM) images which are presented in Fig. 4. UAC technique was being successfully employed for the fabrication of aluminium and magnesium based nanocomposites [46,47,55,58–64].

The SEM image taken on the fractured surface of tensile test specimen fabricated from Al 7075 based nanocomposite is shown in Fig. 5. The fractured surfaces showed considerable dimples and cleavage facets.

2.2. Surface modification of nano-reinforcements

Heating the nano reinforcement particles prior to their inclusion [42] and/or addition of alloying elements like magnesium [65] and calcium [66] have been tried by the researchers to improve the wettability characteristics of nanoparticles. Reinforcement preheating was attempted to remove surface impurities, alter the surface composition and for desorbing the

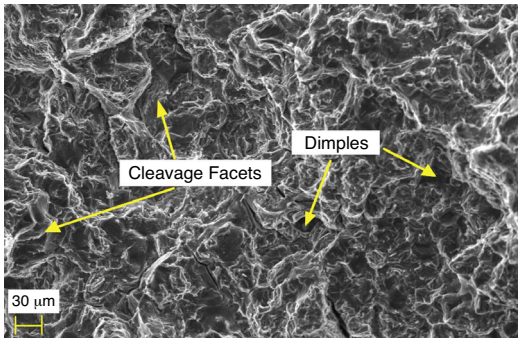

Fig. 5. SEM image of the fracture surface of AL 7075 based nanocomposite [91].

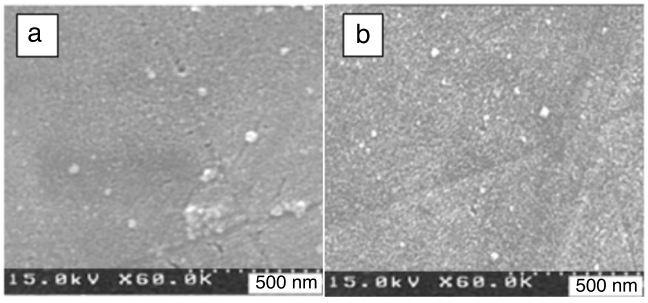

Fig. 6. SEM images of A356 based nanocomposite with (a) Al-Al_2O_3 ball milled powders and (b) Cu-Al_2O_3 ball milled powders [71].

gases. When this is not accomplished, the wettability of reinforcements may get impaired. The ceramic nanoparticles can be coated with a layer of metals like aluminium (Al) and copper (Cu). In order to achieve the metal coating over the nano-ceramic reinforcements, a planetary ball mill can be charged different mass ratio of metallic powders and nanoparticles and milled for a predetermined time. Through this metal coating, the surface tension of ceramic nanoparticles is favourably getting altered in the molten metal [8,67]. Akbari and his fellow researchers [68–71] adopted this technique for the nanoparticles prior to their inclusion in the melt. This was done to alter the surface energies and thus the wetting behaviour of nanoparticles in the molten metal. For the fabrication of A356 based nanocomposites, nano-Al_2O_3 reinforcements were individually mixed with Al and Cu metallic powders in the mass ratio of 1:1. Using a planetary ball mill, this mixture was subjected to milling procedure using the ball to powder ratio of 20:1 for 24 h. The ball milled powders were introduced into the melt just ahead of the stirring process [71]. The SEM image of the nanocomposite with the incorporation of these ball milled powders revealed the uniform distribution of reinforcements in the base matrix. This can be inferred from Fig. 6. Out of the two metallic powders (Al, Cu) considered for coating, the Cu coated Al_2O_3 had been more uniformly distributed than Al coated Al_2O_3 particles. This might have been associated with the improved wettability characteristics.

A laboratory-based test conducted by Leon et al. [72] supports the result of this uniform distribution of Cu-Al_2O_3 in the molten aluminium metal matrix. A sessile drop test conducted at 800 °C revealed that the wettability angle can be reduced to 12.6° at the interface of Cu-Al_2O_3 and molten aluminium which is sub-

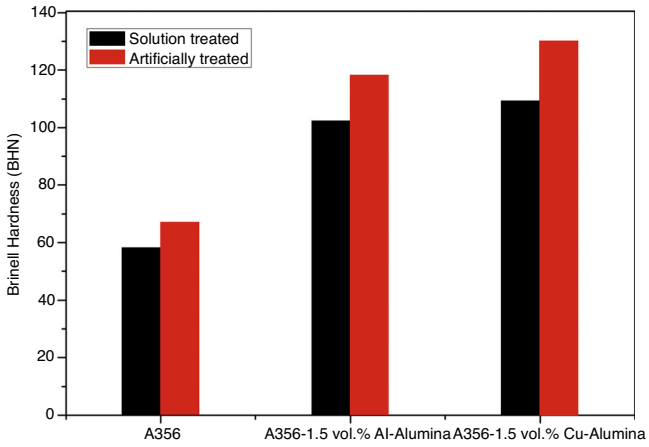

Fig. 7. Effect of ball milled powders on the hardness of the nanocomposite [71].

stantially lower than Al-Al_2O_3 and molten aluminium interface (115.2°). Improved hardness was observed for the composite reinforced with Cu-Al_2O_3 particles over Al–Al_2O_3 particles for the same stirring time of 4 min. This is shown in Fig. 7. A similar trend was observed for other mechanical properties such as 0.2% yield strength (YS), ultimate tensile strength (UTS) and ductility.

2.3. Focus on particle capture in matrix

The strength of van der Waals forces, interaction among the particles and in between the particles and molten metal is decided by Hamaker constant [70,73,74]. Considering a situation, where the ceramic nanoparticles do not make severe chemical reactions with melt (due to its inertness) and subjected to negligible buoyancy and gravity forces, the van der walls energy (E_{vdw}) associated with a single nanoparticle of spherical shape can be given by the following equation:

$$E_{vdw} = -\frac{A_{132}R}{6d_0} \quad (1)$$

where A_{132} – Hamaker constant for substances 1 and 2 in the presence of medium 3; R – radius of the sphere; d_0 – distance between nanoparticle and solidification front. In particle capture system by the solidification front, A_{132} can be described as A_{sys}

$$A_{sys} \approx \left(\sqrt{A_{\text{solid metal}}} - \sqrt{A_{\text{liquid metal}}}\right) \times \left(\sqrt{A_{\text{nanoparticle}}} - \sqrt{A_{\text{liquid metal}}}\right) \quad (2)$$

when the Hamaker constant is greater than zero, the interaction is attractive and it is repulsive, whilst it is less than zero. The lower plasma frequency of liquid metal makes A_{solid} typically higher than A_{liquid}. The van der Waals energy will be positive if $A_{nanoparticles}$ is lower than A_{liquid} and vice versa. The positive van der Waals energy generally has the tendency of pushing the nanoparticles away and thus aids the prevention the agglomeration. Akbari et al. [70] developed aluminium (A356) based composites with the incorporation of TiO_2 and TiB_2 nanoparticles using focus on particle capture in the matrix. Hamaker constant for the different materials used in their investigation is presented in Table 3. Using Eqs. (1) and (2), the A_{sys} and E_{vdw} of any composite systems can be determined. The Al-TiO_2 and Al-TiB_2 composite systems analyzed by Akbari and his co-workers are presented in Table 4.

Table 3
Hamaker constant of main materials [73].

Material	TiB_2	TiO_2	Al (s)	Al (l)
Hamaker constant (zJ)	256	150	333	266

Table 4
Viscous capture of Al-TiO_2 and Al-TiB_2 composite systems [70].

Metal – nanoparticle system	R (nm)	A_{sys} (zJ)	E_{vdw} (J)
Al – TiO_2	20	−7.853	130.883
Al – TiB_2	20	−0.59	9.83

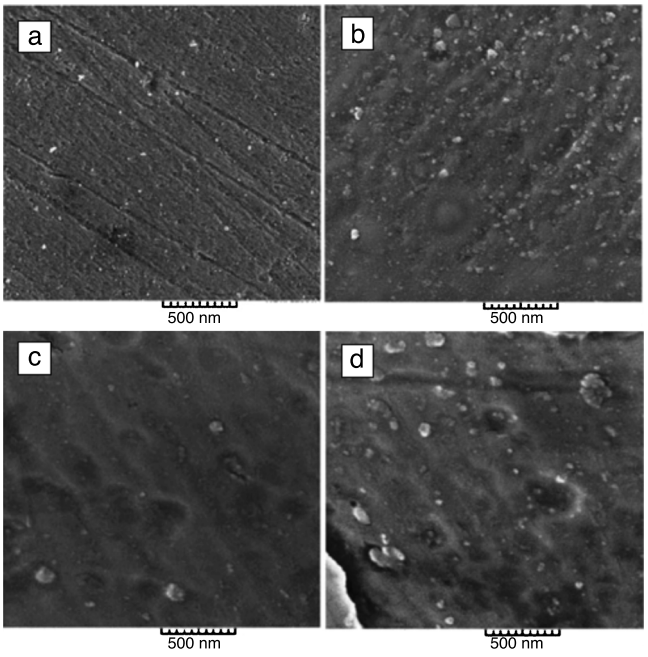

Fig. 8. Particle distribution in (a) 0.5 vol.% TiB_2, (b) 1.5 vol.% TiB_2, (c) 0.5 vol.% TiO_2 and (d) 1.5 vol.% TiO_2 composites [70].

Table 3 shows the Al-TiO_2 system is subjected to higher van der walls energy than Al-TiB_2 composite system. TiO_2 nanoparticles are severely pushed away from the solidification front in Al-TiO_2 than in Al-TiB_2 system. It is also reported that the rejection of nanoparticles is much lower in the Ti-B_2 system. Moreover, the more uniform particle distribution was reported in Al-TiB_2 than Al-TiO_2 composites. This is presented in Fig. 8. Agglomeration was observed in both composite systems, but the magnitude was much lower in Al-TiB_2 composites. The Hamaker constant values are closer for liquid aluminium and TiB_2 particles which result in a favourable condition for particle capture in Al-TiB_2 composite system. Due to this fact, better mechanical properties were observed in A356-TiB_2 composite than A356-TiO_2 for an invariable nanoparticle concentration.

3. Semisolid processing of nanocomposites

The semisolid slurry that has near globular grains and solid fraction within 20–60% can be given a final shape using semisolid processing method. This method is characterized by low porosity and shrinkage. Inherently, a low processing temperature is required for this technique. In addition, the non-turbulent filling can be minimized [75]. The following section throws light on the semisolid processing techniques adopted by the researchers for the fabrication of nanocomposites.

3.1. Compocasting

Compocasting has been attempted by researchers to manufacture aluminium based metal matrix composites, in which nano ceramic reinforcements are added to the semi-solid matrix through mechanical stirring. In compocasting, two processing routes available: viz. semisolid–semisolid (SS) and semisolid–liquid (SL). In both routes, during the mixing of reinforcements, the matrix is in semisolid state. But during casting, the matrix may be partially liquid (SS route) or fully liquid (SL route). Out of these two processing routes, SS route is normally associated with processing difficulties caused by the high viscosity of the matrix under semisolid condition. Moreover, it is difficult to obtain uniform particle distribution and composite with porosity to a lesser extent [4,76]. Thus, SL route compocasting is gaining importance over SS route.

Amirkhanlou and his co-workers [77–80] explored a practical approach called semisolid processing (compocasting) for the fabrication of aluminium composites with a uniform distribution of reinforcement particles in the matrix. Silicon carbide, pure aluminium, and pure magnesium powders (8 μm, 80 μm and 40 μm, resp.) were used as starting materials for preparing three different forms (untreated SiC, ball milled Al-SiC and Al-SiC-Mg) of reinforcement powders. In order to accomplish the comparative evaluation, the composites were developed under both stir-cast (liquid processing) and compo-casting (semisolid processing) conditions. The schematic of the experimental setup used for their investigation is presented in Fig. 9.

For the fabrication of composites, about 1.2 kg of A356 alloy was melted in a graphite crucible using an electric resistance heating element and the temperature of the melt was raised to 700 °C. An electro-mechanical stirrer was made to run 500 rpm for 2 min to ensure the homogeneous temperature of melt prior to the injection of composite powders. Different composites were developed with the injection of all the three different forms of composite powders into the melt. The injection was realized using a carrier gas like argon. For developing composites under stir-cast (liquid state processing) conditions, the melt was cooled and stirred until its temperature drops 650 °C. The molten metal at this temperature was then poured into a die to obtain a casting. Whilst composites under compo-cast (semisolid processing) condition were developed by cooling the melt to 607 °C (corresponding to 0.2 solid fraction according to Scheil equation). An average cooling rate of 4.2 °C/min was adopted for all the experiments.

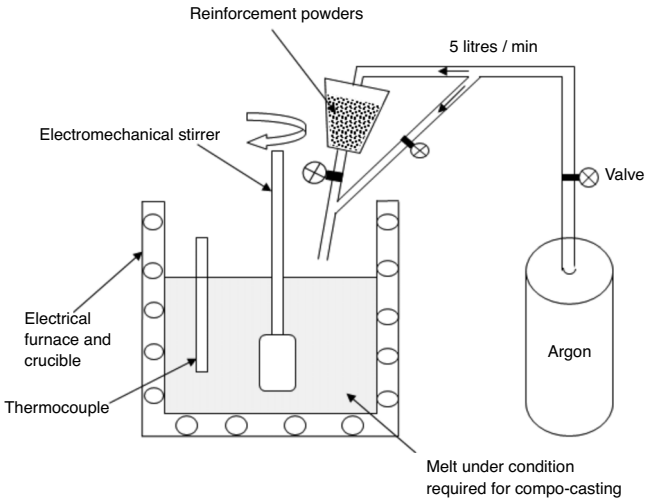

Fig. 9. Experimental set up for semisolid processing of composites [78].

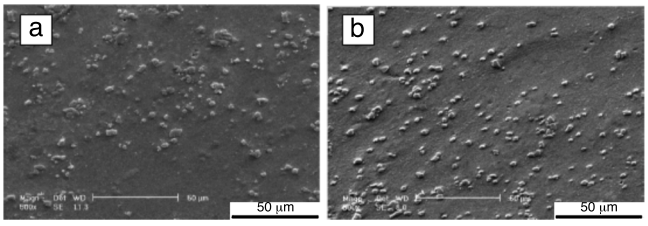

Fig. 10. SEM images of (a) Al356-5% Al coated SiC_p – 650 °C (stir cast) and (b) Al356-5% Al coated SiC_p – 607 °C (compocast) [78].

The microstructural investigation of developed composite samples revealed that the distribution is uniform with ball-milled reinforced powders under semisolid processing than liquid processing route [78]. It is evident from their SEM images shown in Fig. 10 that semisolid processed composite with treated reinforcement powders was found to possess better mechanical properties over stir cast composite with untreated reinforcements. About 5–7% reduction in porosity is observed in compocasting than stir casting [79]. Improved mechanical properties are obtained with compocasting than stir casting. When comparing to stir cast composite, the percentage improvement in mechanical properties of A356-5%SiC_p compocast composite fabricated at room temperature and high temperature is graphically represented in Fig. 11. Nevertheless, the improvement is slightly getting impaired with increasing temperature.

In compo-casting, prior to slurry pouring into the preheated die mould, an appreciable amount of solidification typically happens in the crucible itself, which lowers the slurry temperature than that of stir-casting. As consequence, the solidification shrinkage, hydrogen evolution and air entrapment effects are greatly reduced in compo-casting, which generally results in reduced porosity and thus improved mechanical properties [76–81].

3.2. Rheocasting compounded with squeeze casting

A limited number of research works have been performed on the fabrication of nanocomposites using either rheocasting alone

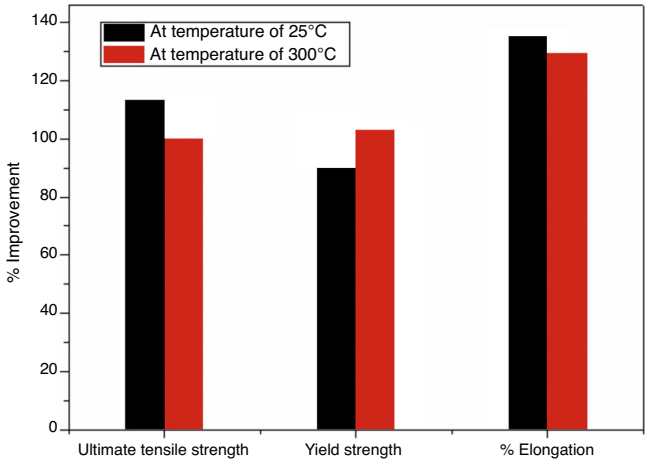

Fig. 11. Percentage improvement in mechanical properties for compocast composites over stir-cast composites at room and elevated temperatures [80].

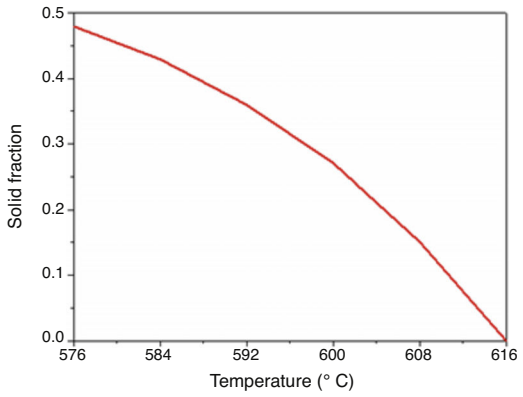

Fig. 12. Temperature vs solid fraction curve of A356 aluminium alloy calculated from DSC [87].

[82–84] or a combination of rheo and squeeze casting [85,86]. Elshalakany et al. [85] fabricated A356 based nanocomposite by reinforcing multiwall carbon nanotubes (MWCNT). In this method, a weighed quantity of A356 alloy was melted in the furnace to 660 °C A solid degasser such as hexachloroethane is added to the melt to prevent degassing and the molten metal is purged with argon gas to prevent hydrogen entrapment during melt processing. The molten alloy was slowly cooled to 601 °C (semisolid state). According to Scheil equation, this is corresponding to solid/liquid fraction of 0.30 for A356 alloy. The temperature Vs solid fraction curve for A356 alloy calculated from differential scanning calorimetry (DSC) analysis is shown in Fig. 12. To the melt, pure magnesium is added to improve the wettability of nano-reinforcements. Magnesium addition is followed by the introduction of nano-reinforcement powders and they are subjected to stirring for a time period of about 1 min under the semisolid state. After the preinfiltration of the preform by the molten metal, it is reheated to 620 °C to form homogeneous mixture and agitation continued for another 1 min. While the molten mixture has attained the temperature of 601 °C, it is poured into the preheated die mould and squeezing pressure is applied during solidification.

Establishment of the non-dendritic semisolid slurry is one of the most critical tasks in rheocasting [88]. Direct ultrasonic vibration (DUV) and indirect ultrasonic vibration (IUV) have been tried by earlier researchers to obtain favourable semisolid slurry [88–90]. In DUV method, after pouring the molten metal into a preheated metal cup, an ultrasonic vibrator is immersed into the melt at 15–20 mm from the surface and operated for 90 s. Then, the semisolid slurry with certain solid fraction was poured into a cold chamber die casting machine. In IUV method, the horn is not making direct contact with molten metal rather it vibrates on the bottom side of the metallic cup containing the melt to prepare the non-dendritic semisolid slurry. The favourable semisolid slurry can be obtained within 50 s, which is considerably less than DUV. Apart from obtaining non-dendritic structures, a promising characteristic of semisolid processing is the minimization of porosity. Complete elimination of porosity through a high pressure die casting (HPDC) is not possible due to the high rate of mould filling. Instead, squeeze casting (SC) can be adopted to address the issues posed by HPDC. Due to the secondary processing such as hot extrusion and squeeze casting, the grains are significantly refined due to dynamic precipitation recrystallization (DRX) and particle stimulation of nucleation (PSN) mechanisms. This leads to further improvement in hardness, yield and ultimate tensile strength [85,86] and impact strength of the composites [91].

3.3. Thixoforming

Thixoforming (TF) is one of the semisolid processing techniques, which essentially composed of three processes viz. feedstock preparation, reheating and forming in the semisolid state [92,93]. Fabrication of thixoformed composites with high solid fraction is preferred as low liquid phase distributed in the composite act as a lubricant to reduce the deformation forces at the interface and also aids in redistribution of reinforcement [94]. Powder thixoforming (PTF) is a variant of TF, which combines the blending and compacting steps of powder metallurgy (PM) with partial remelting and forming processes of thixoforming. Thus, PTF has the potential of attaining the homogeneous distribution of reinforcements and products with complex compositions. Moreover, this method permits the manufacturing of large size complex components by retaining their compact microstructure. The schematic representation of PTF is shown in Fig. 13.

The filling behaviour, final microstructure and thus the terminal properties of TF products are mainly dependent upon the microstructure evolution during the partial remelting process. A lot of research works have been accomplished on the behaviour of aluminium and magnesium alloys [96–99]. Jiang et al. [100] investigated the influence of remelting temperature, soaking time on the microstructure evolution of Al7075-1.5% SiC_p nanocomposite. Initially, with increasing partial remelting temperature, grain coarsening occurs and beyond a certain limit, it starts to reduce. In general, if the grains are not sufficiently round, upon shearing, too much interference will lead to the disappearance of thixotropic behaviour [101]. Hence, roundness factor of less than 2 is preferred [102]. The effect of partial

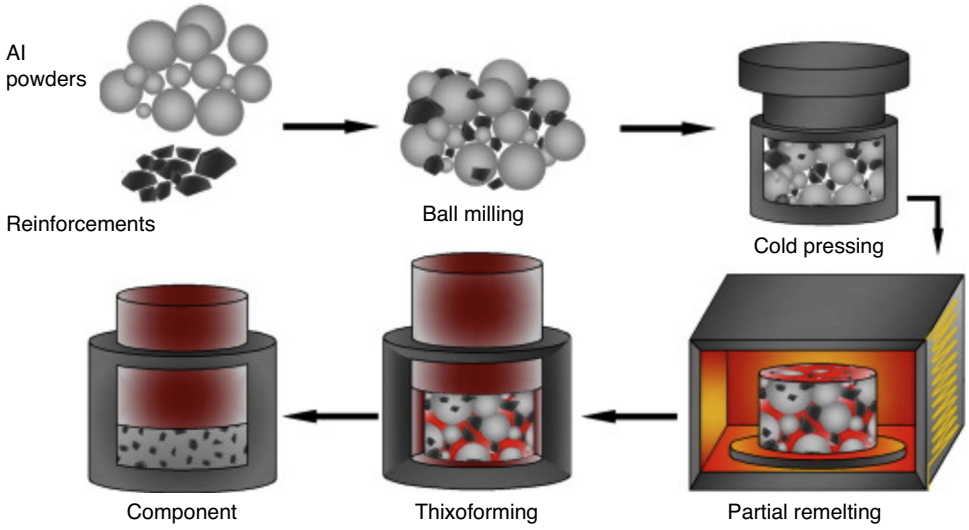

Fig. 13. Schematic representation of powder thixoforming [95].

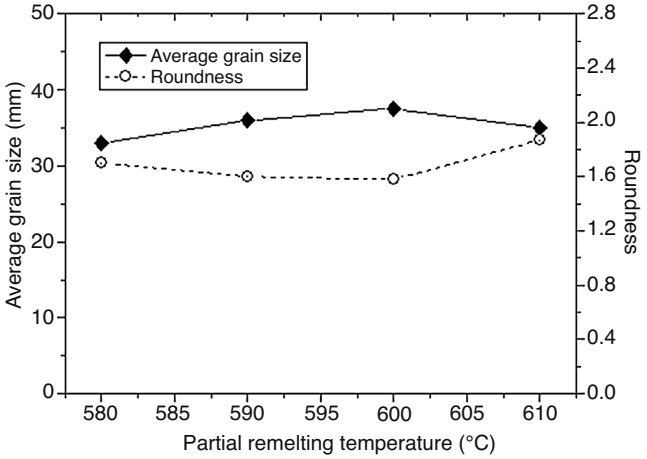

Fig. 14. Effect of partial remelting temperature on the average grain size and roundness [100].

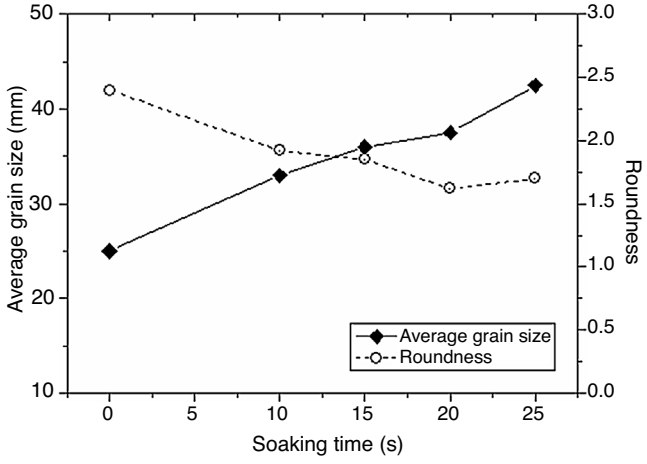

Fig. 15. Effect of soaking time on the average grain size and roundness [100].

remelting temperature and soaking time on the average size of grains and their roundness is presented in Figs. 14 and 15 respectively.

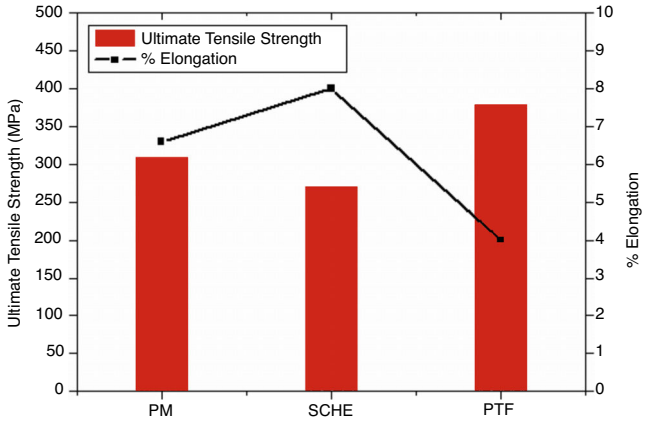

Fig. 16. Comparison of mechanical properties of Al 2024-10% SiC_p fabricated by different methods [95].

Li et al. [95] executed the comparative evaluation of Al 2024-10% SiC_p composite manufactured through different methods, which is shown in Fig. 16. The authors concluded that semisolid processing such as PTF resulted in composites with improved properties over those produced with traditional techniques such as PM, stir casting with hot extrusion (SCHE). It is also inferred that the ductility of the composite can be improved by adopting secondary processing such as extrusion.

4. Infiltration processed nanocomposites

Although infiltration technique can be successfully implemented for the production of Al and Mg-based nanocomposites, their utilization is limited due to long infiltration times and higher cost of preforms. Infiltration technique can be carried out employing either pressure-assisted [103] or pressure less injection of liquid metal [104] into the porous preform. In spite of cost-effectiveness, pressureless infiltration requires long processing time. The preform is prepared from a slurry that consists of a binder, reinforcement phase and liquid carrier that is subsequently subjected to filtration. Thus prepared preform

Table 5
Summary of the influence of different liquid processing techniques on mechanical properties of nanocomposites.

Matrix	Reinforcements	Manufacturing processes	Improvement in properties	Ref.
A356	SiC: 30 nm	Ultrasonic assisted cavitation	Yield strength, ultimate strength and hardness were improved without a compromise on the ductility.	[109]
A356	SiC: 50 nm Al_2O_3: 20 nm	Ultrasonic assisted cavitation	An improvement in tensile strength and % elongation was observed with SiC than Al_2O_3 for the same level of reinforcement.	[110]
AA2024	Al_2O_3: 65 nm	Ultrasonic assisted cavitation	An increase of 37% in UTS and 81% in YS was observed with 1 wt.% reinforcement of Al_2O_3.	[111]
Al 7075	SiC and B_4C: 50 nm	Ultrasonic assisted cavitation	An increase in microhardness and ultimate tensile strength over unreinforced alloy was observed with both SiC and B_4C reinforcements.	[112]
AA6061	B_4C: 50 nm	Ultrasonic assisted cavitation	Uniform dispersion of reinforcement was observed in the matrix. Highest UTS and retained ductility and impact strength were observed with 2 wt.% reinforcement. Better wear resistance was reported for the nanocomposite over monolithic alloy.	[113]
Pure Mg	β-SiC: 50 nm	Ultrasonic assisted cavitation	Higher yield strength and ultimate tensile strength were observed while ductility was retained.	[114]
Pure Al	B_4C: 80 nm	Ultrasonic assisted cavitation	Nanocomposites were exhibiting higher hardness than pure aluminium. Better high temperature wear characteristics were also observed for composites.	[115]
Pure Al	Si_3N_4: 30 nm	Ultrasonic assisted cavitation	Microstructure revealed uniform dispersion of nanoparticles. The yield and tensile strength improved without reducing the thermal conductivity.	[116]
Al-Si-Mg	SiC: 20 nm, 30 nm and 40 nm	Double stir casting	Uniform dispersion of nanoparticles in the matrix was aided by the double stirring technique. Improved tensile strength and ultimate tensile strength were reported.	[117]
A356	MWCNT: 10–30 nm	Compocasting	Better grain refinement, low solidification shrinkage and gas adsorption were reported. Compocast nanocomposites were possessing higher density and hardness than conventional liquid state processed nanocomposites.	[118]
A359	SiC	Rheo-processing with HPDC	Improved wear resistance was reported over unreinforced aluminium alloy.	[119]
A356	Al_2O_3: 20 and 60 nm	Rheocasting with squeeze casting	Better thermal and electrical conductivity were reported with 60 nm reinforcements over 200 nm.	[120]
A413	Mg	Thixoforming	Better wear resistance was reported for thixoformed composite over unreinforced alloy.	[121]
A356	Ni coated SiC (100 PPI)	Vacuum infiltration	Enhanced mechanical and thermal properties were reported.	[122]
Zn	Nanocrystalline SiC (12, 20 nm) Nanocrystalline diamond (5 nm, 16 nm)	High-temperature, high-pressure infiltration	Higher micro-hardness was reported for nanocomposites.	[123]
Al	Reinforcement: B_4C Metal particulates: Ti	Metal-assisted pressureless infiltration	Better flexural, compressive strength and wear resistance were reported for the Al/B_4C composites.	[124]

is completely dried. Further, it is heat treated to achieve dimensional stability during pressure assisted molten metal infiltration. The pictorial representation of infiltration technique is shown in Fig. 17.

Xiong et al. [105,106] produced Al-based nanocomposites with the preform that was made from ball milling and cold pressing of SiC nanoparticles. They adopted the pressureless infiltration. A single stage pressureless infiltration technique was followed for the production of Al-based composites [107]. This infiltration technique is also suitable for the manufacturing Mg-based nanocomposites [108].

Different advanced liquid processing techniques adopted by the researchers for the fabrication of nanocomposites and their influence on mechanical properties is presented in Table 5.

5. Conclusions

In this article, the influence of advanced liquid processing techniques such as ultrasonic assisted cavitation, compocasting, rheocasting, thixoforming and infiltration on the uniform distribution of nanoparticles has been reviewed and presented. Microstructural and mechanical properties of nanocomposites are found to be primarily dependent upon the method of fabrication. Out of these different techniques, the infiltration method is being used in limited applications due to longer processing time and higher cost of preforms. In order to obtain favourable results, the rheocasting should not be used alone, but along with squeeze casting, which in turn increases the manufacturing cost. In semi-liquid processing, powder thixoforming is found

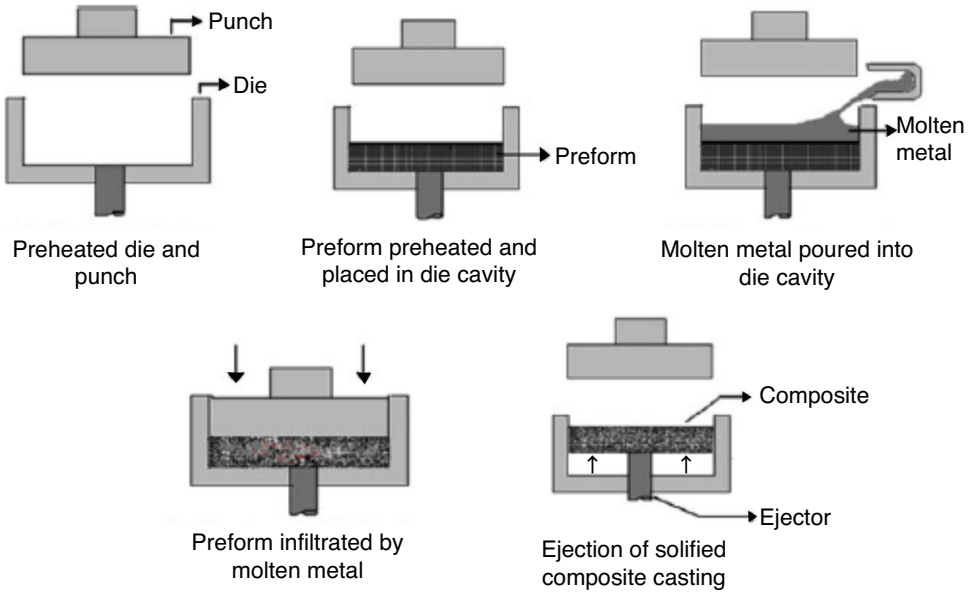

Fig. 17. A pictorial representation of pressure infiltration technique.

to produce nanocomposites with improved mechanical properties higher than powder metallurgy (solid processing route) and stir casting with hot extrusion (liquid processing route). The mechanical properties of nanocomposites produced through compocasting are found to be in the same range of powder thixoforming. But keeping the objectives of low cost, processing time and amount of skill required, ultrasonic assisted cavitation is gaining its importance over other techniques. In addition, the nanocomposites fabricated via this method show a remarkable improvement in hardness, tensile strength, creep behaviour and wear resistance.

References

[1] M.K. Surappa, Sadhana – Acad. Proc. Eng. Sci. 28 (2003) 319.
[2] M.K. Surappa, P.K. Rohatgi, J. Mater. Sci. 16 (1981) 983.
[3] B. Maruyama, AMPTIAC Newslett. 2 (1998) 132.
[4] F. Akhlaghi, A. Lajevardi, H.M. Maghanaki, J. Mater. Process. Technol. 155–156 (2004) 1874.
[5] I. Kerti, F. Toptan, Mater. Lett. 62 (2008) 1215.
[6] L. Ceschini, Aluminum and Magnesium metal matrix nanocomposites, Springer, Singapore, 2017, pp. 19, ISBN: 978-981-10-2680-5.
[7] M.M. Tash, E.R. Mahmoud, Materials 9 (2016) 442.
[8] J. Hashim, L. Looney, M.S. Hashmi, J. Mater. Process. Technol. 119 (2001) 324.
[9] S.I. Oh, J.Y. Lim, Y.C. Kim, J. Yoon, G.H. Kim, J. Lee, Y.M. Sung, J.H. Han, J. Alloys Compd. 542 (2012) 111.
[10] R. Warren, C.H. Anderson, Composites 15 (1984) 101.
[11] J.J. Brennan, J.A. Pask, J. Am. Ceram. Soc. 51 (1968) 569.
[12] D.C. Halverson, A.J. Pyzik, I.A. Aksay, J. Am. Ceram. Soc. 6 (1985) 736.
[13] J.V. Naidich, Prog. Surf. Membr. Sci. 14 (1981) 353.
[14] J.G. Li, Ceram. Int. 20 (1994) 391.
[15] J. Eichler, C. Lesniak, J. Eur. Ceram. Soc. 28 (2008) 1105.
[16] A. Maqbool, M.A. Hussain, F.A. Khalid, N. Bakhsh, A. Hussain, M.H. Kim, Mater. Charact. 86 (2013) 39.
[17] J. Wang, Z. Li, G. Fan, H. Pan, Z. Chen, D. Zhang, Scr. Mater. 66 (2012) 594.
[18] R.S. Rana, R. Purohit, S. Das, Int. J. Sci. Res. Pub. 2 (2012) 1.
[19] B.C. Pai, K.G. Satyanarayana, P.S. Robi, J. Mater. Sci. Lett. 11 (1992) 779.
[20] S. Jayalakshmi, Metallic Amorphous Alloy Reinforcements in Light Metal Matrices, Springer International, 2015, pp. 7, ISBN: 978-3-319-15015-4.
[21] B.S. Yigezu, M.M. Mahapatra, P.K. Jha, J. Miner. Mater. Charact. Eng. 1 (2013) 33948.
[22] D.K. Das, P.C. Mishra, S. Singh, S. Pattanaik, Int. J. Mech. Mater. Eng. 9 (2014) 1.
[23] M. Rosso, J. Mater. Process. Technol. 175 (2006) 364.
[24] T. Varol, A. Canakci, S. Ozsahin, Acta Metall. Sin. 28 (2015) 182.
[25] A. Canakci, H. Cuvalci, T. Varol, F. Erdemir, S. Ozkaya, E.D. Yalcin, Powder Metall. Met. Ceram. 53 (2014) 275.
[26] T. Varol, A. Canakci, J. Alloys Compd. 649 (2015) 1066.
[27] T. Varol, A. Canakci, Met. Mater. Int. 21 (2015) 704.
[28] F. Erdemir, A. Canakci, T. Varol, Trans. Nonferrous Met. Soc. China 25 (2015) 3569.
[29] J. Singh, A. Chauhan, J. Mater. Res. Technol. 5 (2016) 159.
[30] M.O. Bodunrin, K.K. Alaneme, L.H. Chown, J. Mater. Res. Technol. 4 (2015) 434.
[31] G.B. Veeresh Kumar, C.S.P. Rao, N. Selvaraj, J. Miner. Mater. Charact. Eng. 10 (2011) 59.
[32] B.B. Ram, in: RK Everett (Ed.), Metal Matrix Composites: Processing and Interfaces, Academic Press, London, 2012, ISBN: 978-0-12-341832-6.
[33] T.W. Clyne, P.J. Withers, An Introduction to Metal Matrix Composites, Cambridge University Press, 1995, ISBN: 0521483573, 9780521483575.
[34] J. Hashim, L. Looney, M.S. Hashmi, J. Mater. Process. Technol. 92-93 (1999) 1.
[35] A. Canakci, T. Varol, S. Ozsahin, Int. J. Adv. Manuf. Technol. 78 (2015) 305.
[36] A. Canakci, F. Arslan, T. Varol, Sci. Eng. Compos. Mater. 21 (2014) 505.
[37] A. Canakci, S. Ozsahin, T. Varol, Arab. J. Sci. Eng. 39 (2014) 6351.
[38] A. Canakci, F. Arslan, T. Varol, Mater. Sci. Technol. 29 (2013) 954.
[39] S.K. Thandalam, S. Ramanathan, S. Sundarrajan, J. Mater. Res. Technol. 4 (2015) 333.
[40] T.S. Kumar, R. Subramanian, S. Shalini, J. Anburaj, P.C. Angelo, Indian J. Eng. Mater. Sci. 23 (2016) 20.
[41] T. Noguchi, K. Asano, S. Hiratsuka, H. Miyahara, Int. J. Cast. Met. Res. 21 (2008) 219.
[42] S.A. Sajjadi, H.R. Ezatpour, H. Beygi, Mater. Sci. Eng. A – Struct. 528 (2011) 8765.
[43] G. Cao, H. Choi, J. Oportus, H. Konishi, X. Li, Mater. Sci. Eng. A – Struct. 494 (2008) 127.
[44] X. Li, Y. Yang, X. Cheng, J. Mater. Sci. 39 (2004) 3211.
[45] J. Lan, Y. Yang, X. Li, Mater. Sci. Eng. A – Struct. 386 (2004) 284.

[46] Y. Yang, X. Li, J. Manuf. Sci. Eng. 129 (2007) 497.
[47] Y. Yang, J. Lan, X. Li, Mater. Sci. Eng. A – Struct. 380 (2004) 378.
[48] O.V. Abramov, Ultrasound in Liquid and Solid Metals, CRC Press, 1994, ISBN: 9780849393556.
[49] W.L. Nyborg, Physical Acoustics, Academic Press, New York, 1965, pp. 265.
[50] K.S. Suslick (Ed.), Ultrasound: Its Chemical, Physical, and Biological Effects, 6th ed., VCH Publishers, New York, 1988.
[51] K.S. Suslick, Y. Didenko, M.M. Fang, T. Hyeon, K.J. Kolbeck, W.B. Mcnamara, M.M. Mdleleni, M. Wong, Philos. Trans. R. Soc. Lond. A – Math. Phys. Eng. Sci. 357 (1999) 335.
[52] Y. Sunekawa, H. Suzuki, Y. Genma, Mater. Des. 22 (2001) 467.
[53] L. Ma, F. Chen, G. Shu, J. Mater. Sci. Lett. 14 (1995) 649.
[54] D.K. Koli, G. Agnihotri, R. Purohit, Mater. Today Proc. 2 (2015) 3017.
[55] S. Jia, D. Zhang, Y. Xuan, L. Nastac, Appl. Acoust. 103 (2016) 226.
[56] R. Harichandran, N. Selvakumar, Arch. Civil Mech. Eng. 16 (2016) 147.
[57] X. Li, Y. Yang, D. Weiss, Metall. Sci. Technol. 26 (2008) 12.
[58] S. Jia, P.G. Allison, T.W. Rushing, L. Nastac, et al. (Eds.), Advances in the Science and Engineering of Casting Solidification, Springer International, 2015, ISBN: 978-3-319-48605-5.
[59] N. Srivastava, G.P. Chaudhari, Mater. Sci. Eng. A – Struct. 651 (2016) 241.
[60] X.Y. Jia, S.Y. Liu, F.P. Gao, Q.Y. Zhang, W.Z. Li, Int. J. Cast. Met. Res. 22 (2009) 196.
[61] L. Shiying, L. Wenzhen, J. Xiuying, G. Feipeng, Z. Qiongyuan, Rare Met. Mater. Eng. 1 (2010) 029.
[62] R.S. Harini, B. Raj, K.R. Ravi, Trans. Indian Inst. Met. 68 (2015) 1059.
[63] R. Rajeshkumar, V. Udhayabanu, A. Srinivasan, K.R. Ravi, J. Alloys Compd. 726 (2017) 358.
[64] C. Kannan, R. Ramanujam, J. Alloys Compd. 751 (2018) 183.
[65] B.F. Schultz, J.B. Ferguson, P.K. Rohatgi, Mater. Sci. Eng. A – Struct. 530 (2011) 87.
[66] Q.B. Nguyen, M. Gupta, J. Compos. Mater. 43 (2009) 5.
[67] R. Asthana, S.N. Tewari, Compos. Manuf. 4 (1993) 3.
[68] M.K. Akbari, H.R. Baharvandi, O. Mirzaee, Composites Part B – Eng. 52 (2013) 262.
[69] M.K. Akbari, H.R. Baharvandi, O. Mirzaee, J. Compos. Mater. 48 (2014) 3315.
[70] M.K. Akbari, S. Rajabi, K. Shirvanimoghaddam, H.R. Baharvandi, J. Compos. Mater. 49 (2015) 3665.
[71] M.K. Akbari, O. Mirzaee, H.R. Baharvandi, Mater. Des. 46 (2013) 199.
[72] C.A. Leon, G. Mendeza-Suarez, R.A.L. Drew, J. Mater. Sci. 41 (2006) 5081.
[73] J.Q. Xu, L.Y. Chen, H. Choi, X.C. Li, J. Phys.: Condens. Matter 24 (2012) 1.
[74] G. Kaptay, Mater. Sci. Forum 215–216 (467) (1996).
[75] F. Czerwinski, Magnesium Injection Molding, Springer, US, 2008, ISBN: 978-0-387-72399-0.
[76] S.A. Sajjadi, M. Torabi-Parizi, H.R. Ezatpour, A. Sedghi, J. Alloys Compd. 511 (2012) 226.
[77] S. Amirkhanlou, B. Niroumand, Trans. Nonferrous Met. Soc. China 20 (2010) 788.
[78] S. Amirkhanlou, B. Niroumand, Mater. Des. 32 (2011) 1895.
[79] S. Amirkhanlou, B. Niroumand, J. Mater. Eng. Perform. 22 (2013) 85.
[80] S. Amirkhanlou, B. Niroumand, Mater. Sci. Eng. A – Struct. 528 (2011) 7186.
[81] S.A. Sajjadi, H.R. Ezatpour, M.T. Parizi, Mater. Des. 34 (2012) 106.
[82] M. Esmaily, N. Mortazavi, J.E. Svensson, M. Halvarsson, M. Wessen, L.G. Johansson, A.E.W. Jarfors, Composites Part B – Eng. 94 (2016) 176.
[83] M. Esmaily, N. Mortazavi, J.E. Svensson, M. Halvarsson, A.E.W. Jarfors, M. Wessen, R. Arrabal, L.G. Johansson, Mater. Chem. Phys. 180 (2016) 29.
[84] K.S. Alhawari, M.Z. Omar, M.J. Ghazali, M.S. Salleh, M.N. Mohammed, Procedia Eng. 68 (2013) 186.
[85] A.B. Elshalakany, T.A. Osman, A. Khattab, B. Azzam, M. Zaki, J. Nanomater. (2014), http://dx.doi.org/10.1155/2014/386370.
[86] M.T. Parizi, A. Habibolahzadeh, G.R. Ebrahimi, Mater. Sci. Eng. A – Struct. 693 (2017) 33.
[87] H.M. Guo, X.Q. Luo, A.S. Zhang, X.J. Yang, Trans. Nonferrous Met. Soc. China 20 (2010) 1361.
[88] S. Lu, S. Wu, W. Dai, C. Lin, P. An, J. Mater. Process. Technol. 212 (2012) 1281.
[89] S.S. Wu, G. Zhong, W. Li, Ping An, Y.W. Mao, Trans. Nonferrous Met. Soc. China 20 (2010) 763.
[90] S.S. Wu, J.W. Zhao, L.P. Zhang, P. An, Y.W. Mao, Solid State Phenom. 141-143 (2008) 451.
[91] C. Kannan, R. Ramanujam, J. Adv. Res. 8 (2017) 309.
[92] M.R. Rokni, Z. Zarei-Hanzaki, H.R. Abedi, N. Haghdadi, Mater. Des. 36 (2012) 557.
[93] A. Bolouri, M. Shahmiri, C.G. Kang, J. Alloys Compd. 509 (2011) 402.
[94] S.J. Qu, A.H. Feng, L. Geng, Z.Y. Ma, J.C. Han, Scr. Mater. 56 (2007) 951.
[95] P.B. Li, T.J. Chen, H. Qin, Mater. Des. 112 (2016) 34.
[96] A. Bolouri, M. Shahmiri, C.G. Kang, J. Mater. Sci. 47 (2012) 3544.
[97] H.S. Kim, I.C. Stone, B. Cantor, J. Mater. Sci. 43 (2008) 1292.
[98] Z. Zhao, Q. Chen, Y. Wang, D. Shu, Mater. Sci. Eng. A – Struct. 506 (2009) 8.
[99] S. Kleiner, O. Beffort, P.J. Uggowitzer, Scr. Mater. 51 (2004) 405.
[100] J. Jiang, Y. Wang, X. Nie, G. Xiao, Mater. Des. 96 (2016) 36.
[101] S. Ji, Z. Fan, M.J. Bevis, Mater. Sci. Eng. A – Struct. 299 (2001) 210.
[102] M. Kiuchi, R. Kopp, CIRP Ann. Manuf. Technol. 51 (2002) 653.
[103] S.W. Lai, D.D.L. Chung, J. Mater. Sci. 29 (1994) 3128.
[104] S.M. Zhou, X.B. Zhang, Z.P. Ding, C.Y. Min, G.L. Xu, W.M. Zhu, Composites Part A – Appl. Sci. Manuf. 38 (2007) 301.
[105] B. Xiong, Z. Xu, Q. Yan, C. Cai, Y. Zheng, B. Lu, J. Alloys Compd. 497 (2010) 1.
[106] B. Xiong, Z. Xu, Q. Yan, B. Lu, C. Cai, J. Alloys Compd. 509 (2011) 1187.
[107] A. Bahrami, M.I. Pech-Canul, N. Soltani, C.A. Gutierrez, P.H. Kamm, A. Gurlo, J. Alloys Compd. 694 (2017) 408.
[108] J.S. Babu, K.P. Nair, G. Unnikrishnan, C.G. Kang, H.H. Kim, J. Compos. Mater. 44 (2010) 971.
[109] S. Donthamsetty, D. Nageswara Rao, DIU J. Sci. Technol. 5 (2010) 48.
[110] X. Liu, S. Jia, L. Nastac, Int. J. Met. Cast. 8 (2014) 51.
[111] H. Su, W. Gao, Z. Feng, Z. Lu, Mater. Des. 36 (2012) 590.
[112] S. Gopalakannan, T. Senthilvelan, J. Sci. Ind. Res. 74 (2015) 281.
[113] L. Poovazhagan, K. Kalaichelvan, T. Sornakumar, Mater. Manuf. Process. 31 (2016) 1275.
[114] G. Cao, H. Konishi, X. Li, Int. J. Met. Cast. 2 (2008) 57.
[115] R. Harichandran, N. Selvakumar, G. Venkatachalam, Trans. Ind. Inst. Met. 70 (2017) 17.
[116] F. He, E. Forthofer, Int. J. Met. Cast. 5 (2011) 71.
[117] V.S. Aigbodion, Recent Pat. Nanotechnol. 5 (2011) 234.
[118] B. Abbasipour, B. Niroumand, M.S.M. Vaghefi, Trans. Nonferrous Met. Soc. China 20 (2010) 1561.
[119] U.A. Curle, L. Ivanchev, Trans. Nonferrous Met. Soc. China 20 (2010) 852.
[120] E.S. El-Kady, T.S. Mahmoud, A.A. Ali, Mater. Sci. Appl. 2 (2011) 1180.
[121] H. Saghafian, S.G. Shabestari, M.H. Ghoncheh, F. Sahihi, Tribol. Trans. 58 (2015) 288.
[122] D. Cree, M. Pugh, J. Mater. Process. Technol. 210 (2010) 1905.
[123] S. Gierlotka, B.F. Palosz, A. Swiderska-Sroda, E. Grzanka, G. Kalisz, K. Fietkiewicz, S. Stelmakh, C. Lathe, Solid State Phenom. 101–102 (2005) 157.
[124] Y.T. Yao, L.Q. Chen, Mater. Manuf. Process. 31 (2016) 1286.